https://doi.org/ 10.15407/ujpe68.6.412

SADEQ H. LAFTA

University of Technology – Iraq
(Baghdad, Iraq; e-mail: sadeqhlafta@uotechnology.edu.iq)

INVESTIGATION OF THE STATIC SHEAR STRESS IN A SUSPENSION OF $Co_{0.2}Ni_{0.8}Fe_2O_4$ NANOPARTICLES IN SESAME OIL

Spinel ferrite nanoparticles of $Co_{0.2}Ni_{0.8}Fe_2O_4$ composition are utilized as filler magnetic particles in the carrier fluid of sesame oil to prepare a magnetorheological fluid. The hydrothermal method is adopted to prepare CoNi ferrite nanoparticles. X-ray diffraction analysis is used to check the crystalline phase, and transmission electron microscopy is used to image the particles to find the size and shape of particles. The average size is about 18 nm. The magnetic properties are determined by measuring the hysteresis loop by the superconducting quantum interference device technique. The saturation magnetization is 59.4 emu/g, and the coercivity is 30 Oe. The Langevin fitting is applied to the hysteresis loop to show that the particle moment is about $16 \times 10^3 \mu_B$. The viscosity and shear stress are measured against the shear rate, where the latter parameters are extracted from the viscosity and the viscometer spindle speed. The viscosity behavior showed the shear thinning against the shear rate. The viscosity increases with the magnetic field. The shear stress increases with the shear rate and has a very good matching with the Bingham model, rather than with the Herschel–Bulkley model, while describing the measured data. We observed a clear high static shear stress at low shear rates that are growing with the magnetic field. The yield stress was increased linearly with magnetic field strength.

Keywords: $Co_{0.2}Ni_{0.8}Fe_2O_4$, magnetorheological fluid, magnetic properties, static shear stress, yield shear stress, shear thinning.

1. Introduction

There is always a necessity for modern materials that are used to do a significant function in enhancing the human health and life modality. Smart materials can do these functions. The new smart materials should have some features such as safety, good quality, reliability, and green as much as possible. Smart materials must have a high response to the control signals to modify their properties. In addition, smart materials should have stable properties to help one in designing the innovative systems with various applications [1]. One of the most important smart materials is a magnetorheological fluid (MRF) [2]. MRF is usually composed mainly of a carrier fluid such as a synthesized oil, and micro-size magnetic particles commonly carbonyl iron in micron size, where the larger particle size will support the chains. However, there is a chance to prepare a magnetizable colloidal or MRF with ferrite nanoparticles with unique magnetorheological properties, sometimes called ferrofluid [3]. De-

Citation: Lafta Sadeq H. Investigation of static shear stress in a suspension of $Co_{0.2}Ni_{0.8}Fe_2O_4$ nanoparticles in sesame oil. *Ukr. J. Phys.* **68**, No. 6, 412 (2023). https://doi.org/10.15407/ujpe68.6.412.

Цитування: Лефта Садек Х. Дослідження статичного зсувного напруження в суспензії $Co_{0,2}Ni_{0,8}Fe_2O_4$ наночастинок у кунжутній олії. *Укр. фіз. журн.* **68**, №6, 413 (2023).

spite MRF with large iron particles (>1 μm) having a stronger yield stress, two orders of kPa, compared to a fluid containing iron oxide particles with nanoparticles (<100 nm) about one order of kPa. On the other hand, MRF with nanoparticles is more stable due yo a high dispersivity. Besides, the nanoparticles are less abrasive [4].

Magnetorheological fluid (MRF) as a significant smart material has different applications in different fields and is continuously developed; they are involving automation, aerospace, the manufacturing industry, and medical application. The common MRF devices are the MRF damper (shock absorber), brake, clutch, mount, prosthetic leg, lower-limb exoskeleton, hydraulic pump, lubrication, MRF valve [5], MRF brake, MRF seals, MRF pneumatic actuator, MRF polishing, MRF fixture, seismic isolators, and exercise equipment [6].

MRF usually functions in the post-yield zone (not the pre-yield zone), i.e., the stress is larger than the yield stress, where the stress depends on the magnetic field greatly. In this zone, the MRF is used mainly in the dampers to absorb vibrations, vehicle suspension development, and seat suspension implementation [7]. While in the pre-yield zone, the MRF must have low viscosity, as it is known by off-state [6].

When fluids flow, they may behave themselves like the Newtonian fluid or non-Newtonian one. The non-Newtonian flow means that the viscosity depends on time and displays a special relationship between the shear rate and shear stress. One of these special relations or manners is the shear thinning. The shear thinning means reducing the apparent viscosity, as the shear rate is rising. The larger the shear rate, the lower the viscosity. Furthermore, the shear thickening means an increase in the apparent viscosity associated with the shear rate increases. The larger the shear rate, the higher the viscosity [8]. Fluids that show the shear thinning are also known as pseudoplastic fluids. They are commonly complex fluids like blood and MRF. Despite the behavior is not fully realized, it is commonly treated as a result of the microstructural ordering in the fluid. The shear Thinning is frequently accompanied by other effects like the heating or nonlinear high shear stress [9].

Away from Newtonian fluids, by approaching the non-Newtonian fluids, those fluids have some "static viscosity", i.e., a minimum shear stress before it starts to flow, which obeys the Bingham plastic model [10]. It depends on the apparent viscosity and experimental temperature [11], which can be measured by a bench-top tuning fork viscometer and a magnetometer in view of vsrious factors that affect the rheological properties of MRF like magnetic particle fraction, carrier fluid and particle densities, particle size [12], particle shape, their distribution, and physical properties of the carrier fluid [13], as well as additional additives, exerted magnetic field, and temperature [14]. Some of the factors are typically necessary to increase the yield stress; such as increasing the volume fraction of MR particles and/or increasing the exerted magnetic field strength [15]. Sometimes, these techniques may be considered undesirable, because they may add a sensible weight to the MRF devices and increase the off-state viscosity of MRF [16].

$NiFe_2O_4$ nanoparticles were synthesized by the gel burning method and showed the ferromagnetic nature of their magnetic properties as measured by a vibrating sample magnetometer. The $NiFe_2O_4$ nanoparticles were utilized in the preparation and characterization of MRF. The viscosity was raised by an increase in the magnetic flux density. There was an enhancement in the yield stress with an increase in the particle content and also an increase in the viscosity due to the dipole–dipole interactions of magnetic nanoparticles. The behavior of MRF was explained basing on the Bingham plastic model [17]. In another study, Co ferrite was added in different ratios to the Li grease. The off-state viscosity of MR grease was measured, and these particles showed a decrease in the off-state viscosity with increasing the magnetic field. The magnetorheology grease samples with concentrations of Co ferrite in the interval 1–5 wt.%, were tested by SEM, a vibrating sample magnetometer, and a rheometer. The MR grease samples showed that, at the addition of 5 wt.% Co ferrite powder, the initial off-state viscosity was decreased by 86% with respect to the pure MR grease. The initial viscosity of MR grease grew, when the field is raised to 0.64 T, as the amount of Co ferrite nanoparticles is increased. In addition, an improvement in the shear stress and yield stress was observed, as the Co ferrite content is increased compared to the reference MR grease sample [18]. In work [19], Co ferrite nanoparticles were precipitated on multiwall carbon nanotubes using the co-precipitation technique. The produced composite samples were used as filling magnetic particles for

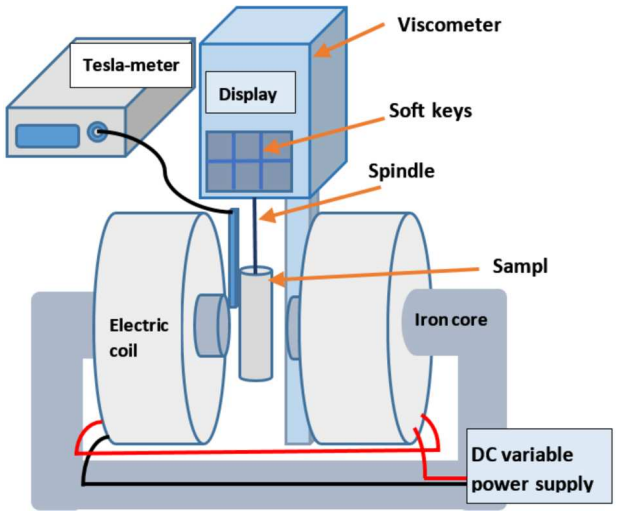

Fig. 1. The viscosity measurement setup using visco basic plus rotational viscometer

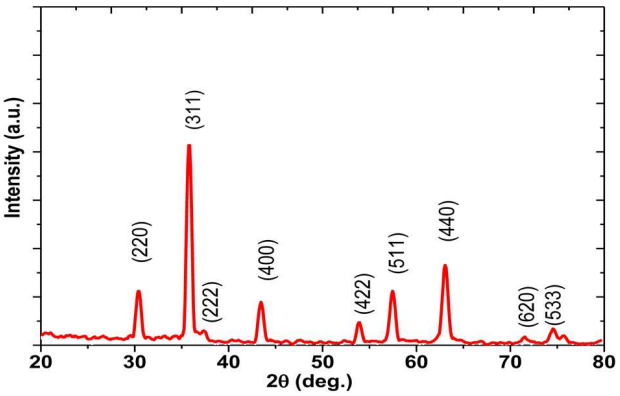

Fig. 2. The XRD pattern of the prepared $Co_{0.2}Ni_{0.8}Fe_2O_4$

preparing a magnetorheological fluid. The viscosity, shear stress, yield stress, storage modulus, and loss modulus were found to depend mainly on the applied magnetic fields.

In this study, a $Co_{0.2}Ni_{0.8}Fe_2O_4$ ferrite was prepared, and its structural and magnetic properties were determined. Then an MR fluid was prepared by mixing these particles with sesame oil to investigate the magnetorheological properties and exactly the static shear stress. It is the first time to check the magnetorheological properties of such a suspension. The novelty is also concentrated on sensing and investigating the static shear stress experimentally at a low shear rate, which was not measured previously as far as the author knows.

2. Experimental Part

2.1. Sample preparation

Hydrothermal synthesis was adopted to prepare the ferrite nanoparticles. The analytical grade precursors $NiCl_2 \cdot 6H_2O$, $CoCl_2$, and $FeCl_3$ have weights of 0.52 g, 2.08 g of $NiCl_2 \cdot 6H_2O$, and 6.48 g of $FeCl_3$, respectively. Distilled water (DW) of a volume of 150 ml was used as a solvent. After the mixing, the salt with DW for 10 min, the aqueous NaOH solution of 0.25 M concentration was added very slowly in the form of drops to the salt solution up to the pH reaches 7, accompanied by a robust stirring. Then the product was transferred to a Teflon cup in a stainless container and heated to 160 °C for 4h by a hotplate. After the power was off, the suspension was left to reach room temperature on the second day. The suspension was washed three times with DW and one time with ethanol to remove the salts and any organic residuals. As a final step, the suspension was dried at about 70 °C to get the final black powder with a noticeable attraction to the magnet.

The powder sample was checked by the XRD Expert Panalytical Diffractometer to identify the crystalline phase. To analyze the particle image, the Philips CM12 TEM was utilized. The magnetization-field curve was obtained by Quantum Design MPMS XL SQUID. Sesame oil supplied from Kadoya/Japan was used as a carrier fluid. The ferrite weight of 1.9152 g was mixed with 1.123 g of oleic acid supplied by Hebei Guanlang Biotechnology Co in an ultrasonic bath. Then it was dried with ethanol to remove the extra oleic acid. After that, the oleic-coated ferrite is mixed with 5 g sesame oil by the strong magnetic stirring for 20 min and then in an ultrasonic bath for 2h to achieve a good dispersion and the mixing of ferrite particles in the sesame oil. VISCO BASIC PLUS ROTATIONAL was used to measure the magnetorheological properties. Figure 1 illustrates the magnetorheological measurement setup. The magnetic field was measured by PHYWE digital Tesla meter.

3. Results and Discussion

3.1. Structural Properties

In Fig. 2, the X-ray diffraction (XRD) pattern of the prepared $Co_{0.2}Ni_{0.8}Fe_2O_4$ sample is presented. The base solution acts to yield metal hydroxides that subsequently are converted to ferrite during the drying process. This action can be summarized through the

Table 1. **Some crystalline parameters that are related to the XRD pattern for the prepared $Co_{0.2}Ni_{0.8}Fe_2O_4$ sample**

The lattice constant (a), Å	The XRD density, g/cm^3	The average crystallite size (t), nm	Hoping length (S_A), Å	Hoping length (S_B), Å	Dislocation density (d_d), line/m^2
8.34	5.31	13	3.63	2.95	2.26×10^{15}

following chemical reaction:

$$0.2CoCl_2 + 0.8NiCl_2 \cdot 6H_2O + 2FeCl_3 + 8NaOH \rightarrow$$
$$\rightarrow Co_{0.2}Ni_{0.8}Fe_2O_4 + 8NaCl + 8.8H_2O. \quad (1)$$

The pattern of the sample matches the 044–1485 card of the spinel ferrite that is related to the symmetry family of Fd-3m, where the main seven peaks of the sample match the mentioned card peaks. Table 1 shows some extracted parameters that are related to the XRD pattern. The average crystallite size (t) is smaller than ferrite crystals synthesized by different chemical routes [20–23], while it can be considered close to other ferrite crystals [21] and larger than other ferrites [24]. The tolerance in the crystal sizes is related mainly to the different preparation conditions and the difference in the compositions [25]. The lattice constant (a) value is in between that for Ni ferrite and Co ferrite [26]. The XRD density is in agreement with the other studies [27], and it is considered a high density due to the suitable preparation conditions that were chosen.

The hoping lengths for tetrahedral S_A and octahedral S_B sites are calculated using Eq. (2) [28] and given in Table 1. We have

$$S_A = \sqrt{3}\frac{a}{4} \text{ and } S_B = \sqrt{2}\frac{a}{4}. \quad (2)$$

The S_A and S_B parameters represent the distance between the magnetic ions, and they are slightly larger than for Ni ferrite, which may not degrade the magnetic properties through reducing the interaction between these ions [29]. To calculate the dislocation density (d_d) in line/m^2 of the synthesized $Co_{0.2}Ni_{0.8}Fe_2O_4$ nanoparticles, Eq. (3) was used [30], and the result is shown in Table 1. The parameter (d_d) influences the magnetization by reducing the anisotropy constant [31]

$$d_d = 1/t^2 \quad (3)$$

The ionic radii of Co^{2+}, Fe^{3+}, and Ni^{2+} are 0.745 Å, 0.60 Å, and 0.69 Å, respectively. This may be the reason for that the lattice constant of these particles is greater than for Ni ferrite ones (8.31 Å) [26].

In Fig. 3, *a* and *b*, the TEM images of the synthesized particles are shown. Images (*a*) and (*b*) illustrate that particles have spherical shapes. The particle size is ranging from about 8 to about 70 nm,

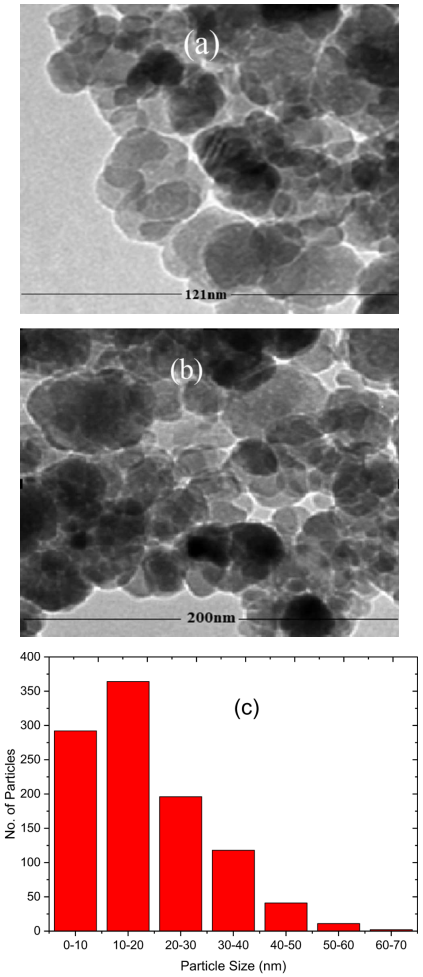

Fig. 3. The (*a*) and (*b*) sub-figures are the TEM images of the prepared $Co_{0.2}Ni_{0.8}Fe_2O_4$ nanoparticles. The particle size distribution of the synthesized particles (*c*)

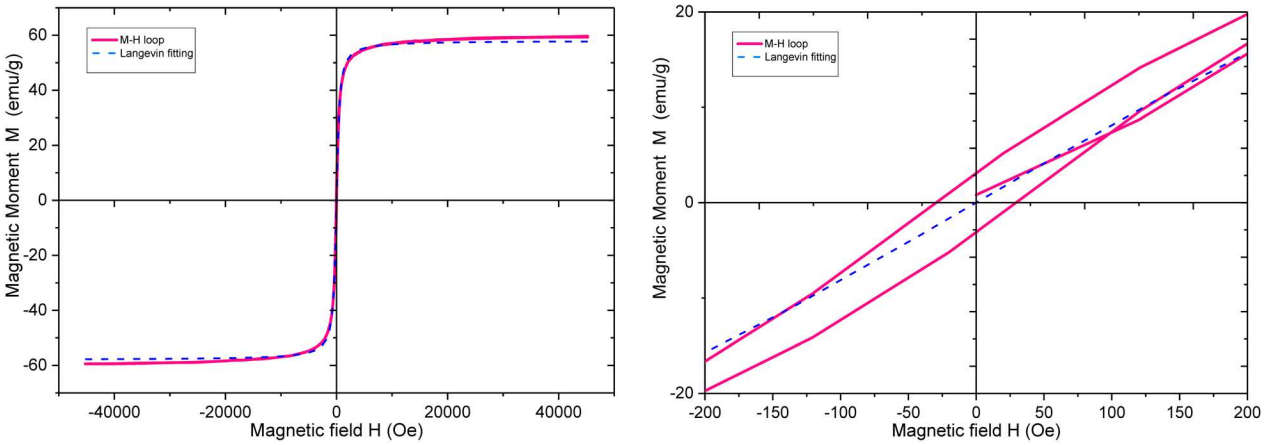

Fig. 4. Magnetic hysteresis loop with its Langevin fitting in (a), and the low-field area to illustrate the intersection with axes in (b)

Table 2. **Extracted magnetic parameters of the synthesized $Co_{0.2}Ni_{0.8}Fe_2O_4$ ferrite nanoparticles**

Magnetization saturation M_s (emu/g)	Coercivity H_c (Oe)	Remanent magnetization M_r (emu/g)	Squareness ratio M_r/M_s	Initial permeability μ_i (emu/g · Oe)	Anisotropy constant K_{an} (emu · Oe/g)
59.4	30	2.6	0.0437	0.0771	891

where most particles are around 18 nm, as is illustrated in Fig. 3, c, where the particle size distribution is given. As the particle size is larger than the crystallite size, this supports that particles are mostly polycrystalline, especially the large ones, which explains, in turn, the spherical shape of the particles.

3.2. Magnetic hysteresis characterization

The magnetic hysteresis loop of the prepared particles is shown in Fig. 4, *a*. The prepared $Co_{0.2}Ni_{0.8}Fe_2O_4$ ferrite nanoparticles show a normal soft hysteresis with (s) shape. Figure 4, *b* displays the magnification of the low-field region, around the origin, of the loop. The magnetic parameters are shown in Table 2. The magnetization saturation M_s (59.4 emu/g) is higher than in workss [28] and [30], but it is comparable to the ones of [32] and [33]. The measured coercivity H_c, which is 30 Oe, is considered a low value compared to that of other nanoparticles prepared by other techniques [34]. The small H_c value occurred despite that the cobalt increases the coercivity of Ni ferrite nanoparticles [35]. It is believed that this gives an indication that particles are always superparamagnetic ones. This analysis may be supported by the measured particle size, where too many particles have an average size lower than 25 nm for Co ferrite [36, 37] and 15 nm for Ni ferrite [34]. The remanence magnetization is 2.6 emu/g, which is lower than that given in [25]. The squareness ratio is low due to the high M_s and low remanence. The anisotropy constant is given by Eq. (4) [38]:

$$K_{an} = H_c M_s/2. \tag{4}$$

The calculated magnitude of K_{an} is 891 emu · Oe/g (5.4×10^3 erg/cm^3), it is much lower than K_{an} of bulk Co ferrite (2×10^6 erg/cm^3) and for nano Co ferrite 3.7×10^5 erg/cm^3 and higher than for Ni ferrite (5×10^3 erg/cm^3) [39], where K_{an} is enlarged, as the Co content is increased [40].

In ferrimagnetic materials, the saturation magnetization is superexchange interaction dependent between tetrahedral sites and octahedral sites [41]. So, cations (Co^{2+} and Ni^{2+}) and their content at these sites contribute directly to the Ms. Co^{2+} prefers oc-

Table 3. **The fitting and calculated magnetic parameters**

The fitting saturation magnetization (M_s)	Particle moment (m_p)	The estimated particle (D_e)	The experimental magnetic moment (μ_{exp})
58.04 emu/g	$16 \times 10^3 \mu_B$	11 nm	2.45 μ_B

cupying A sites, but occupying B sites is possible, while Ni^{2+} prefers occupying B sites. On the other hand, Fe^{3+} can be in both sites. Co^{2+} ions also tend to both sites Co^{2+} mostly substitutes Ni^{2+}, when it entered the lattice. This may be accompanied by Fe^{3+} migration to the B sites, which, in turn, raises the magnetization of the B sublattice. This distribution is responsible for having such respectively high-value M_s [42].

The Langevin fitting for the measured loop provides a useful information about the magnetic saturation and particle moment [43]. The fitting Langevin equation is given in Eq. (5) [44]:

$$M(H,T) = M_s \left[\coth\left(\frac{m_p H}{k_B T}\right) - \left(\frac{k_B T}{m_p H}\right)\right], \tag{5}$$

where $M(H,T)$ is the magnetization at any field (H) and temperature (T), m_p is the particle moment. The blue dashed line in Fig. 3 shows the Langevin fitting curve for the measured $Co_{0.2}Ni_{0.8}Fe_2O_{4\,4}$ ferrite loop, as it was done by OriginLab software. The results showed that M_s equals 58.04 emu/g and m_p of about $19.41 \times 10^3 \mu_B$. The measured particle moment is comparable to that for nano Co ferrite in [45] and [46], which is $16 \times 10^3 \mu_B$, but it is lower than for magnetite [47].

The estimated particle size in terms of the particle moment and magnetization saturation is [44]:

$$D_e^3 = \frac{6 m_p}{M_s \pi}. \tag{6}$$

According to Eq. (5) the estimated particle size is about 11nm. This value is within the interval fo particle sizes that was measured by TEM, but it is less than the average particle size. It is believed that this difference is attributed to the accuracy of the fitting analysis.

The experimental magnetic moment can be found in Eq. (7) [48]:

$$\mu_{\text{exp}} = M_w \times M_s / 5585, \tag{7}$$

where M_w represents the molecular weight, and the resulting moment is in units of μ_B. Using the molecular weight of $Co_{0.2}Ni_{0.8}Fe_2O_4$ as 234.418 g/mol, the latter formula gives a net moment of 2.45 μ_B. It is clear that μ_{exp} follows M_s, as seen in Eq. (7). It is less than that of the Co ferrite, Ni ferrite, and $Co_{0.5}Ni_{0.5}Fe_2O_4$ [46]. Table 3 shows the fitting and calculated parameters.

3.3. Magnetorheological characterization

The used viscometer measures the viscosity as a function of the spindle speed. The speed is transformed to the shear rate via Eq. (8):

$$\gamma\bullet = \frac{\nu}{r_s}, \tag{8}$$

where ν is the spindle speed, and r_s is the spindle radius. The value of r_s is 2 mm. On the other hand, the stress was found from the equation [49]:

$$\tau = \eta\,\gamma. \tag{9}$$

Figure 5 shows the measured viscosity versus the calculated shear rate at different magnetic fields (0–85 mT). All samples are non-Newtonian liquids, and all viscosity curves at different magnetic fields show

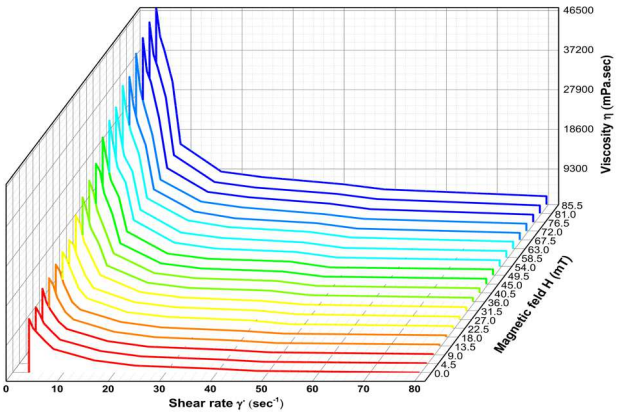

Fig. 5. The measured viscosity-shear rate behavior at different magnetic fields

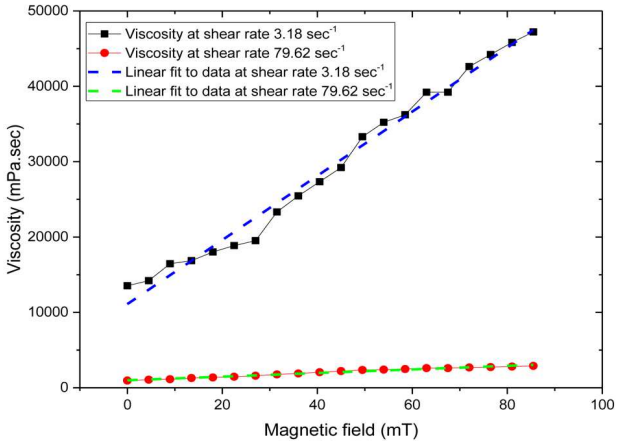

Fig. 6. The measured viscosity as a function of the magnetic field at a low shear rate (3.18 sec^{-1}), and at a higher shear rate (79.62 sec^{-1})

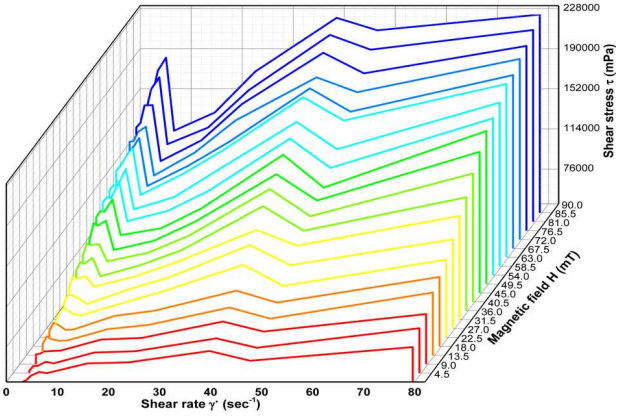

Fig. 7. The shear stress as a function of the shear rate at different magnetic fields

an exponential decrease, as the shear rate increases according to Eq. (9) and as the reflux to the shear-thinning behavior. At the low shear rate and low spindle speed, it is clear that, as the magnetic field increases from zero to 85 mT, the viscosity is increased about 5 times, as seen clearly in Fig. 6. While at a high shear rate of 79.62 sec^{-1} and a high speed such as 100 rpm, the impact of a magnetic field on the viscosity is found to be less than at low shear rate. The slopes of the linear fitting to the viscosity at a shear rate of 4 sec^{-1} and a shear rate of 80 sec^{-1} are significantly different, where the former is about 410 $\text{Pa} \cdot \text{sec/T}$, while the latter is just 23 $\text{Pa} \cdot \text{sec/T}$. This may be attributed to the effect of the magnetic field on the static viscosity rather than the dynamic

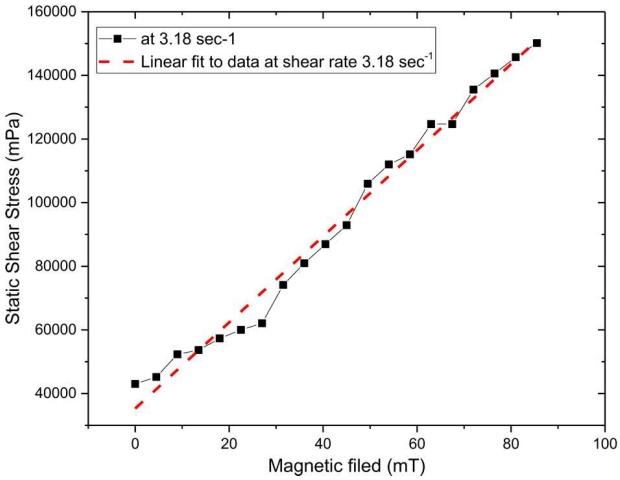

Fig. 8. The shear stress as a function of the magnetic fields at a low shear rate of 3.18 sec^{-1}

one. It was found that this linear behavior tends to be saturated at higher magnetic fields, larger than 400 mT in work [50]. Of course, this depends on some other parameters like the particle fraction.

Jianrong *et al.* [51] showed the manner of the viscosity of such fluid (Fig. 6) by supposing that, at low shear rates, the magnetorheological fluid has a large viscosity, because the magnetic particles have a disorganized arranging that displays a larger motion impedance. While this impedance is reduced, as the shear rates are greater as a result of the particle arrangement in the shear rate orientation. Viscosity was reduced, as a result of the magnetic particles' organized arrangement [52]. The MRF viscosity is influenced by the original viscosity of the oil and the particle fraction [53]. The more the particle content, the more the MRF viscosity [54–55].

Figure 7 illustrates the shear stress variation as a function of the shear rate at different magnetic fields. The first note is that, despite the behavior at a low shear rate, the curves generally again show the clear shear thinning behavior [54], where the stress increases exponentially, as the shear rate increase at each magnetic field strength. This behavior was also shown in some studies such as [55], [56], and [57]. The second note is that, for all curves, the points of each viscosity curve are increased, as the magnetic field is increased as a result of the apparent viscosity increasing [57]. The magnetic field increasing works on making the magnetic chain structure of the MRF thicker and more stable [58], which resists the externally ap-

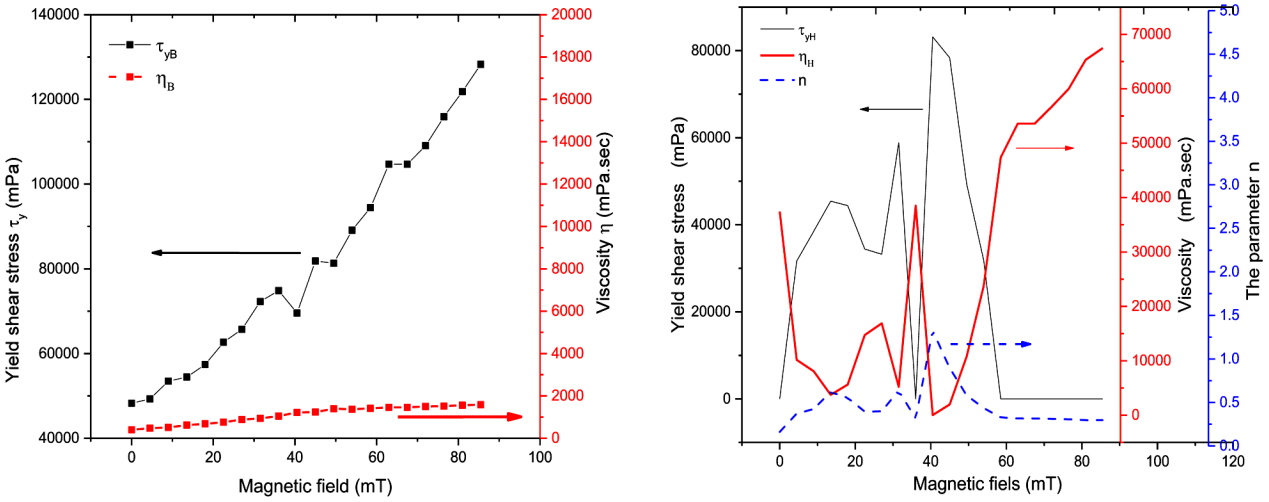

a *b*

Fig. 9. Fitting parameters of the Bingham and the Herschel models as a function of the magnetic fields

plied stress [59]. The third note is the existence of a clear static shear stress at low shear rate values followed by an abrupt decrease, as the shear rate increases, and follows the shear thinning behavior. The static behavior of the shear stress versus the magnetic field is illustrated in Fig. 8. Figure 8 shows the linear relation of the static shear stress with the magnetic field giving a slope of 1353 Pa/T. Again, indeed, the stress is expected to be saturated at ultrahigh fields, as was mentioned previously about the viscosity. It is believed that nanoparticles have a lower response than microparticles [60], which may reduce the rearranging of the nanoparticles again in the chain beyond the static shear rates.

Different models (Bingham model and plastic Herschel–Bulkley, Cross, and Carreau ones) were utilized to understand the manner of this fluid. The three latter models showed the same behavior. So, the Herschel model was chosen to express the others. As a result, the Bingham model and Herschel model have been tried by the Originlab software for each curve in Fig. 7, i.e., at each magnetic field strength. The fitting process was applied after neglecting the point with distinguished high static shear stress values. The equations of the Bingham model and Herschel model are given in the equations below [61]

$$\tau = \tau_{yB} + \eta\gamma, \tag{10}$$

$$\tau = \tau_{yH} + \eta\,(\gamma)^n, \tag{11}$$

where τ_{yB} (or τ_{yH}) equal $\tau_0(H)$ sign(γ) are the yield shear stress caused by a magnetic field. The subscript symbols B and H are standing for the Bingham or Herschel model, $\tau_0(H)$ is the shear stress that depends on the magnetic field (H), the sign is the signum function, and η represents the MRF viscosity. The parameter $\tau_0(H)$ can be expressed by [63]:

$$\tau_0(H) = \tau_0 + \alpha H^{\beta}, \tag{12}$$

where H is the applied magnetic field intensity, α and β are fitting parameters, and τ_0 is the zero-field yield stress of the MRF.

Figure 9 presents the fitting parameters that resulted from the Bingham model and Herschel–Bulkley model in Fig. 9, *a* and Fig. 9, *b*, respectively. The high fluctuations in some parameters for the Herschel model may result from the not-good matching between the experimental data and the model. On another hand, the parameters that resulted from the Bingham model show very low fluctuations and a good computation accuracy against a magnetic field; besides, they show a simple calculation method. For the Bingham model, it is clear that there is a linear dependence between the yield stress (τ_{yB}) and the magnetic field within the tested range of magnetic fields. The linear dependence between the shear stress and the shear rate was found also in [64] and [65] up to the 0.86-T magnetic field strength. The Bingham yield stress is about 1.5 times the one of the Herschel model, while the viscosity in the Herschel model is higher than that in the Bingham model.

For Fig. 9, *b* presenting the fitting in the Herschel–Bulkley model, it can be found that the parameter (n) is less than 1, which represents the shear thinning state. The state of shear thickening is described by $n > 1$. When $n = 1$, the Herschel model will be similar to the Bingham model. Below τ_y, the MR fluid acts as a viscoelastic fluid, but it works as a Newtonian fluid, when $\tau > \tau_y$.

In the Bingham plastic model, when the magnetic field is applied, the ferrite particles in the fluids are aligned in chains [66]. As the movement begins, the chains between the oil layers begin to be broken and cannot be built up simultaneously. This leads to a reduction in the shear stress. At an increase in $\dot{\gamma}$, i.e., at increasing the spindle speed, new chains are created by the applied field H, and the viscosity is lowered. At a specified $\dot{\gamma}$, the rate of chains' breaking will balance the rate of creating them, and the stress will be nearly constant, as one can see from the shear stress curves at the high shear rates in Fig. 7. In this study, the analysis of the MRF behavior shows the high static stress at a low shear rate, where it is believed that this behavior is related to the relatively high ferrite content that works on building the strong particle interactions, and the more number of chains parallel to the applied field are formed, which impedes the fluid movement. This appeared interaction clearlys at the higher magnetic fields. Particle interactions are grown, as the magnetic field is increased to produce a strong chain structure resulting in an increase in the shear stress [67].

4. Conclusion

Nanoparticles of $Co_{0.2}Ni_{0.8}Fe_2O_4$ can have a relatively high magnetization saturation with good values of the other magnetic parameters, and the superparamagnetic particles can be produced by the hydrothermal synthesis at relatively low temperatures. A good fitting between the experimental data and the Langevin equation is observed, when using the hysteresis loop. The magnetorheological characteristics of $Co_{0.2}Ni_{0.8}Fe_2O_4$ ferrite in sesame oil show a Bingham behavior, as fitted by the Bingham model with a shear thinning manner for such MRF smart material. The viscosity shows a normal exponent drop with increasing the shear rate according to the shear thinning behavior. The new observation of this prepared magnetorheological fluid is its high static shear stress, which is increased from the normal value according to the Bingham curve up to 3 times, as the magnetic field is increased from zero to about 85 mT.

The author did not receive support from any organization for the submitted work. The author has no relevant financial or non-financial interests to disclose.

1. T.Ramakrishnan, S.S. Kumar, S.J. S.Chelladurai, S. Gnanasekaran, S. Sivananthan, N.K. Geetha, R. Arthanari, G.B. Assefa. Recent developments in stimuli responsive smart materials and applications: An overview. *J. Nanomaterials* **2022** (Hindawi Limited, 2022).
2. M. Dassisti, G. Brunetti, Magnetorheological fluid applications. *Encyclopedia of Smart Materials* **5**, 260 (2022).
3. M. Molazemi, H. Shokrollahi, B. Hashemi. The investigation of the compression and tension behavior of the cobalt ferrite magnetorheological fluids synthesized by coprecipitation. *J. Magnetism and Magnetic Materials* **346**, 107 (2013).
4. A.G. Olabi, A. Grunwald. Design and application of magneto-rheological fluid. *Materials & Design* **28** (10), 2658 (2007).
5. D.X. Phu, S.-B. Choi. Magnetorheological fluid based devices reported in 2013–2018: Mini-review and comment on structural configurations. *Frontiers in Materials* **6**, 1 (2019).
6. J.S. Kumar, P.S. Paul, G. Raghunathan, D.G. Alex. A review of challenges and solutions in the preparation and use of magnetorheological fluids. *Intern. J. Mechanical and Materials Engineering* **14** (1), 13 (2019).
7. X. De-kui, N. Song-lin, J. Hui, Y. Fang-long. Characteristics, optimal design, and performance analyses of MRF damper. *Shock and Vibration* **2018**, 17 (2018).
8. M.N. Wall. *Understanding Shear Thinning Using Brownian Dynamics Simulation.* B.Sc. Thesis (University of Tennessee at Chattanooga, 2021).
9. P. Vergne. *23 – Super Low Traction under EHD & Mixed Lubrication Regimes.* Ed. by A. Erdemir, J.-M. Martin (Elsevier, 2007).
10. I. Lee, K. Park, J. Lee. Note: Precision viscosity measurement using suspended microchannel resonators. *Rev. Sci. Instruments* **83** (11), 116106 (2012).
11. I. Lee, J. Lee. Quality factor and vibration amplitude based viscosity measurements using suspended microchannel resonators. *Sensors* 1–4, *IEEE, Taipei, Taiwan* (2012).
12. N. Izumo, A. Koiwai, D. Division. Technological background and latest market requirements concerning "Static Viscosity" measurement with a tuning-fork vibration viscometer. In: *Proceeding of Asia-Pacific Symposium on Measurementt of Mass, Force, and Tourqe (APMF 2009)*, June, 1–4, Tokyo, Japan (2009).

13. K. Shah, S.B. Choi. The influence of particle size on the rheological properties of plate-like iron particle based magnetorheological fluids. *Smart Materials and Structures*, **24** (1), 015004 (2015).
14. R. Chen, M.G. Christiansen, P. Anikeeva. Maximizing hysteretic losses in magnetic ferrite nanoparticles *via* model-driven synthesis and materials optimization. *ACS Nano*, **7** (10), 8990 (2013).
15. J.R. Morillas, J. de Vicente. Magnetorheology: A review. *Soft Matter*, **16** (42), 9614 (2020).
16. S.E. Premalatha, R. Chokkalingam, M. Mahendran. Magneto mechanical properties of iron based MR fluids. *American J. Polymer Sci.* **2** (4), 50 (2012).
17. P. Yagnasri, N. Seetharamaiah, U.S. Pantangi. Experimental investigation of nickel ferrite ($NiFe_2O_4$)-based nano-magnetorheological fluid characteristics using MR damper under triangular displacement excitation. *J. Vibration Engineering & Technologies* **10** (7), 2823 (2022).
18. S.M.A. Tarmizi, N.A. Nordin, S.A. Mazlan, N. Mohamad, H.A. Rahman, S.A.A. Aziz, N. Nazmi, M.A. Azmi. Incorporation of cobalt ferrite on the field dependent performances of magnetorheological grease. *J. Mater. Res. Technol.* **9** (6), 15566 (2020).
19. M.M. Mubasher. Nanocomposites of multi-walled carbon nanotubes/cobalt ferrite nanoparticles: synthesis, structural, dielectric and impedance spectroscopy. *J. Alloys and Compounds* **866**, 158750 (2021).
20. R.S. Puche, M.J.T. Fernández, V.B. Gutiérrez, R. Gómez, V. Marquina, M.L. Marquina, J.L.P. Mazariego, R. Ridaura. Ferrites nanoparticles MFe_2O_4 (M = Ni and Zn): hydrothermal synthesis and magnetic properties. *Boletín de La Sociedad Española de Cerámica y Vidrio* **47** (3), 133 (2008).
21. A. Aimable, B. Xin, N. Millot, D. Aymes. Continuous hydrothermal synthesis of nanometric BaZrO3 in supercritical water. *J. Solid State Chem.* **181** (1), 183 (2008).
22. P. Pulišová, J. Kováč, A. Voigt, P. Raschman. Structure and magnetic properties of Co and Ni nano-ferrites prepared by a two step direct microemulsions synthesis. *J. Magnetism and Magnetic Materials* **341**, 93 (2013).
23. S. Verma, P.A. Joy. Magnetic properties of superparamagnetic lithium ferrite nanoparticles. *J. Appl. Phys.* **98** (12), 124312 (2005).
24. J.H. Lee, C.K. Kim, S. Katoh, R. Murakami. Microwave-hydrothermal versus conventional hydrothermal preparation of Ni- and Zn-ferrite powders. *J. Alloys and Compounds* **325** (1–2), 276 (2001).
25. S.H. Lafta. *Preparing Painting Material from Li–Ni Ferrite with Isovalent Substitution.* PhD Thesis (Al-Nahrain University, 2016)
26. S.H. Lafta. Impact of Ni $^{2+}$ content on broadband ferromagnetic resonance of superparamagnetic Ni ferrite (Having Fe^{2+})-epoxy composite. *IEEE Transactions on Magnetics* **54** (9), 1 (2018).
27. W.M. Desoky, J. Gutierrez, M.S. ElBana, T.A. Elmoslami. Exploring the impact of nickel doping on the structure and lowtemperature magnetic features of cobalt nanospinel ferrite. *Appl. Phys. A* **128**, 846 (2022).
28. L.H. Abdel-Mohsen, S.H. Lafta, M.Sh. Hashim. Magnetic properties of Ba ferrite substituted by low fraction of Ni cations. *Kuwait J. Sci.* **50** 3A, 1 (2023).
29. S.N. Dipali, V.J. Swati, Vi.M. Khot, R.A. Bohara, C.K. Hong, S.S. Mali, S.H. Pawar. Cation distribution, structural, morphological and magnetic properties of $Co_{1-x}Zn_xFe_2O_4$ (x = 0–1) nanoparticles. *RSC Adv.* **5**, 2338 (2015).
30. V.A. Bharati, S.R. Patade, S. Bajaj, R. Parlikar, A.P. Keche, V.V. Sondur. Structural and magnetic properties of nickel ferrite nanoparticles prepared by solution combustion method. *J. Phys.: Conference Series* **1644** (1), 012005 (2020).
31. A. Seeger. The effect of dislocation on the magnetization curves of ferromagnetic crystals. *J. Phys. Colloques* **27**, 68 (1966).
32. C. Dong, G. Wang, D. Guo, C. Jiang, D. Xue. Growth, structure, morphology, and magnetic properties of Ni ferrite films. *Nanoscale Res. Lett.* **8** (1), 196 (2013).
33. A. Kumar, N. Yadav, D.S. Rana, P. Kumar, M. Arora, R.P. Pant. Structural and magnetic studies of the nickel doped $CoFe_2O_4$ ferrite nanoparticles synthesized by the chemical co-precipitation method. *J. Magnetism and Magnetic Materials* **394**, 379 (2015).
34. S. Balideh, A. Aavazpour, G. Rezaei, A. Nikzad. Structural and magnetic properties of spinel nickel-cobalt ferrite nanoparticles substituted by dysprosium cation synthesized by hydrothermal method. *Acta Physica Polonica A* **140** (1), 14 (2021).
35. M .Kishimoto, H. Latiff, E. Kita, H. Yanagihara. Structure and magnetic properties of Co–Ni spinel ferrite particles synthesized via co-precipitation and hydrothermal treatment at different temperatures. *Materials Transactions* **60** (4), 485 (2019).
36. F. Alahmari, M.A. Almessiere, Y. Slimani, H. Güngüneş, S.E. Shirsath, S. Akhtar, M. Jaremko, A. Baykal. Synthesis and characterization of electrospun $Ni_{0.5}Co_{0.5-x}Cd_xNd_{0.02}Fe_{1.78}O_4$ nanofibers, *Nano-Structures & Nano-Objects* **24**, 100542 (2020).
37. M. George, A.M. John, S.S. Nair, P.A. Joy, M.R. Anantharaman. Finite size effects on the structural and magnetic properties of sol–gel synthesized $NiFe_2O_4$ powders. *J. Magnetism and Magnetic Materials* **302** (1), 190 (2006).
38. V.K. Chakradhary, A. Ansari, M.J. Akhtar. Design, synthesis, and testing of high coercivity cobalt doped nickel ferrite nanoparticles for magnetic applications. *J. Magnetism and Magnetic Materials* **469**, 674 (2019).
39. K.S. Rao, S.V.R. Nayakulu, M.C. Varma, G.S.V.R.K. Choudary, K.H. Rao. Controlled phase evo-

lution and the occurrence of single domain $CoFe_2O_4$ nanoparticles synthesized by PVA assisted sol-gel method. *J. Magnetism and Magnetic Materials* **451**, 602 (2018).
40. V.H. Ojha, K.M. Kant. Temperature dependent magnetic properties of superparamagnetic $CoFe_2O_4$ nanoparticles. *Physica B: Condensed Matter*, **567**, 87 (2019).
41. A. Zubair, Z. Ahmad, A. Mahmood, W.C. Cheong, I. Ali, M.A. Khan, A.H. Chughtai, M.N. Ashiq. Structural, morphological and magnetic properties of Eu-doped $CoFe_2O_4$ nano-ferrites. *Results in Physics* **7**, 3203 (2017).
42. T. Dippong, E.A. Levei, I.G. Deac, I. Petean, O. Cadar. Dependence of structural, morphological and magnetic properties of manganese ferrite on Ni–Mn substitution. *Intern. J. Molecular Sci.* **23** (6), 3097 (2022).
43. H .Jalili, B. Aslibeiki, A.G. Varzaneh, V.A. Chernenko. The effect of magneto-crystalline anisotropy on the properties of hard and soft magnetic ferrite nanoparticles. *Beilstein J. of Nanotechnology* **10**, 1348 (2019).
44. E.K. Al-Shakarchi, S.H. Lafta, A.M. Musa, M. Farle, R. Salikov. Effect of Ni content on structural and magnetic properties of Li–Ni ferrites nanostructure prepared by hydrothermal method. *J. Superconductivity and Novel Magnetism* **29** (4), 923 (2016).
45. M.C. Varma, G. Choudary, A.M. Kumar, K.H. Rao. Estimating the cation distributions in $Ni_{0.65}Zn_{0.35}Co_xFe_2O_4$ ferrites using X-ray, FT-IR, and magnetization measurements. *Phys. Res. Intern.* **2014**, 1 (2014).
46. S.H. Lafta. Hydrothermal temperature influence on magnetic and FMR properties of hematite nanoparticles. *Surface Rev. Lett.* **29** (07), (2022).
47. M. Zhang, Q. Liu. Solvothermal synthesis and magnetic properties of monodisperse $Ni_{0.5}Zn_{0.5}Fe_2O_4$ hollow nanospheres. *High Temperature Materials and Processes* **38** (2019), 76 (2019).
48. D .Zákutná, D. Nižňanský, L.C. Barnsley, E. Babcock, Z. Salhi, A. Feoktystov, D. Honecker, S. Disch. Field dependence of magnetic disorder in nanoparticles. *Phys. Rev. X* **10** (3), 031019 (2020).
49. C.R. Stein, M.T.S. Bezerra, G.H.A. Holanda, J. André-Filho, P.C. Morais. Structural and magnetic properties of cobalt ferrite nanoparticles synthesized by co-precipitation at increasing temperatures. *AIP Advances* **8** (5), 056303 (2018).
50. Z. Laherisheth, K. Parekh, R.V. Upadhyay. The effect of magnetic field on the structure formation in an oil-based magnetic fluid with multicore iron oxide nanoparticles. *J. Nanofluids* **7** (2), 292 (2018).
51. A. Kolhatkar, A. Jamison, D. Litvinov, R. Willson, T. Lee. Tuning the magnetic properties of nanoparticles. *Intern. J. Mol. Sci.* **14** (8), 15977 (2013).
52. J.L. Ortiz-Quiñonez, U. Pal, M.S. Villanueva. Structural, magnetic, and catalytic evaluation of spinel Co, Ni, and Co–Ni ferrite nanoparticles fabricated by low-temperature solution combustion process. *ACS Omega* **3** (11), 14986 (2018).
53. A. Druc, A. Dumitrescu, A. Borhan, V. Nica, A. Iordan, M. Palamaru. Optimization of synthesis conditions and the study of magnetic and dielectric properties for $MgFe_2O_4$ ferrite. *Open Chemistry* **11** (8), 1330 (2013).
54. M. Kubík, J.Válek, J. Žáček, F. Jeniš, D. Borin, Z. Strecker, I. Mazůrek. Transient response of magnetorheological fluid on rapid change of magnetic field in shear mode. *Sci. Rep.* **12** (1), 10612 (2022).
55. N.V. Quoc, L.D. Tuan, L.D. Hiep, H.N. Quoc, S.B. Choi. Material characterization of MR fluid on performance of MRF based brake. *Frontiers in Materials* **6**, 1 (2019).
56. J. Liu, X. Wang, X. Tang, R. Hong, Y. Wang, W. Feng. Preparation and characterization of carbonyl iron/strontium hexaferrite magnetorheological fluids. *Particuology* **22**, 134 (2015).
57. G. Schramm. *A practical approach to rheology and rheometry* 2nd Edition, Thermo Electron (Karlsruhe) GmbH, Germany, (2004).
58. D. Utami, S.U. Mazlan, F. Imaduddin, N. Nordin, I. Bahiuddin, S. Abdul Aziz, N. Mohamad, S.-B Choi. Material characterization of a magnetorheological fluid subjected to long-term operation in damper. *Materials*, **11** (11), 2195 (2018).
59. L. Pei, H. Pang, X. Ruan, X. Gong, S. Xuan. Magnetorheology of a magnetic fluid based on Fe_3O_4 immobilized SiO_2 core–shell nanospheres: Experiments and molecular dynamics simulations. *RSC Advances* **7** (14), 8142 (2017).
60. V. Chauhan, A. Kumar, N.A. Bhalla, M. Danish, V. Ranjan. Numerical study of shear thickening fluid with distinct particles dispersed in carrier fluid. *Vibroengineering PROCEDIA*, **21**, 242 (2018).
61. M. Wei, K. Lin, L. Sun. Shear thickening fluids and their applications. *Materials & Design* **216**, 110570 (2022).
62. G.R. Peng, W. Li, T.F. Tian, J. Ding, M. Nakano. Experimental and modeling study of viscoelastic behaviors of magneto-rheological shear thickening fluids. *Korea-Australia Rheology J.* **26** (2), 149 (2014).
63. V. Sokolovski, T. Tian, J. Ding, W. Li. Fabrication and characterisation of magnetorheological shear thickening fluids. *Frontiers in Materials* **7** (2020).
64. C. Liu, J. Xie, D.Cai. Analysis and experimental study on rheological performances of magnetorheological fluids. *Mechanics* **26** (1), 31 (2020).
65. R. Ahamed, M.M. Ferdaus, Y. Li. Advancement in energy harvesting magneto-rheological fluid damper: A review. *Korea-Australia Rheology J.* **28** (4), 355 (2016).
66. M. Zubieta, S. Eceolaza, M.J. Elejabarrieta, M.M. Bou-Ali. Magnetorheological fluids: characteriztion and modeling of magnetization. *Smart Materials and Structures* **18** (9), 095019 (2009).
67. N.M. Wereley, A. Chaudhuri, J.H. Yoo, S. John, S. Kotha, A. Suggs, R. Radhakrishnan, B.J. Love, T.S. Sudarshan. Bidisperse magnetorheological fluids using Fe particles at nanometer and micron scale. *J. Intelligent Material Systems and Structures* **17** (5), 393 (2006).

Received 05.05.23

Садек Х. Лефта

ДОСЛІДЖЕННЯ СТАТИЧНОГО ЗСУВНОГО НАПРУЖЕННЯ В СУСПЕНЗІЇ $Co_{0,2}Ni_{0,8}Fe_2O_4$ НАНОЧАСТИНОК У КУНЖУТНІЙ ОЛІЇ

Магнітні феритні наночастинки $Co_{0,2}Ni_{0,8}Fe_2O_4$ із структурою шпінелі використано як наповнювач у кунжутній олії для створення магнітнореологічної рідини. Для отримання наночастинок використовується гідротермальний метод. Рентґенівський дифракційний аналіз використовується для тестування кристалічної фази, а трансмісійна електронна мікроскопія застосовується для визначення розміру та форми частинок. Середній розмір частинок становить близько 18 нм. Магнітні властивості визначаються шляхом вимірювання петлі гістерезису за допомогою техніки надпровідного квантового інтерференційного пристрою. Показано, що в'язкість та зсувне напруження залежать від швидкості зсуву. Поведінка в'язкості свідчить про наявність зсувного розрідження, що залежить від швидкості зсуву. В'язкість зростає з магнітним полем. Зсувне напруження зростає зі швидкістю зсуву і добре узгоджується з моделлю Бінґема, а не з моделлю Гершеля–Балклі. Спостерігається високе значення статичного зсувного напруження для низьких швидкостей зсуву, яке зростає з магнітним полем. Межа плинності зростає лінійно з напруженістю магнітного поля.

Ключові слова: $Co_{0,2}Ni_{0,8}Fe_2O_4$, магнітореологічна рідина, магнітні властивості, статичне зсувне напруження, межа плинності, спричинене зсувом розрідження.